Electronic Supplementary Material (ESI) for Soft Matter.

Electronic Supporting Information

Multifunctional Liquid Marbles to Stabilize and Transport Reactive Fluids

Lankipalli Harsha,[a] Tamanna Bhuyan,[b] Surjendu Maity,[b] Pranab K Mondal,[a] Siddhartha Sankar Ghosh,[b,c] and Dipankar Bandyopadhyay [b,d]*

[a]Department of Mechanical Engineering, Indian Institute of Technology Guwahati, Assam - 781039, India.
[b]Centre for Nanotechnology, Indian Institute of Technology Guwahati, Assam-781039, India.
[c]Department of Biosciences and Bioengineering, Indian Institute of Technology Guwahati, Assam-781039, India.
[d]Department of Chemical Engineering, Indian Institute of Technology Guwahati, Assam - 781039, India.

*E-mail of Corresponding Author: dipban@iitg.ac.in

1. Methodology

1.1 Selection of non-wetting powder for robust LMs

To figure out the endurance of LMs, two different coatings of equivalent masses (3-4 g) were used to compare the stability of H_2O_2 droplet (20 µL, 50 %) with hydrophobic toner ink particles under ambient conditions. These includes coating hydrated magnesium silicate powder and *Lycopodium* grains + talc powder. A rectangular trench was made on glass slide and was filled with 3-4 g of powder to form a hydrophobic bed. LMs were fabricated by rolling a 20 µL droplet of H_2O_2 (50% v/v) on the layer of hydrophobic particles. The mixture of *Lycopodium* grains was prepared (20% w/v) and the solutions were kept in hot air oven for about 5 – 6 h for drying. The dried residue obtained was ground into a fine powder using a mixer. The formation of the liquid marble was captured using a Sony HRD camcorder. The hydrophobicity of magnesium silicate, *Lycopodium* grains plus talc mixture and toner ink particles coating the LMs was compared by measuring the apparent contact angles of marbles against solid particulate supports using ImageJ software. The morphology of larger clumps of toner ink was observed by FESEM analysis. Presence of traces elemental of silicon and carbon was also confirmed from FETEM mapping and EDX analysis. SAED and DLS analysis has been performed to find out the nature and zeta potential of toner particles.

1.2 Iodometric Titration

The amount of H_2O_2 present in the LM was calculated using Iodometric titration.[1] 20µl of H_2O_2 (50%) was withdrawn from the marble between initial and final time intervals of the experiment using a syringe. The collected H_2O_2 solution was put in a vial containing 8 mL of sulphuric acid (H_2SO_4) that oxidizes iodide to iodine in the presence of H_2SO_4. The concentration of potassium iodide (KI) to be added was calculated according to stoichiometric equation. The reaction led to the formation of iodine, which can be seen as a black colored precipitate.

$$H_2O_2 + 2\ KI + H_2SO_4 \rightarrow I_2 + K_2SO_4 + 2\ H_2O \qquad (1)$$

Spectrophotometric estimation of iodine by relating with the concentration of potassium triiodide (KI_3) that was formed by adding an excess amount of KI in the reaction mixture.[2] The formation of KI_3 was required due to insolubility of iodine in water.

$$KI + I_2 \rightarrow KI_3 \qquad (2)$$

The absorbance intensity was directly correlated with the concentration of KI_3.

1.3 Stability of H_2O_2 inside the LM

The stability of H_2O_2 in toner ink armored LMs was tested by studying the reaction between 20% H_2O_2 microdroplet inside LM and 0.2 M KI solution. The activity of H_2O_2 was tested by placing it in a petridish filled with 3 mL of 0.2 M KI solution as a strong catalyst and stored at room temperature undisturbed. The decomposition of H_2O_2 droplet inside the micro reservoir was investigated by the generation of oxygen bubbles in the solution captured using a Sony HRD camcorder.

1.4 Evaporation studies of water droplet

The evaporation parameters along with the buckling time have been measured from images of LM captured using a Sony HRD camcorder. In the case of water droplet evaporation (control), a 20µl droplet of water was dispensed on a glass substrate with small amount of toner ink (10-15 mg) sprinkled on its surface to ensure formation of a spherical shape such that we could relate its volume with the marble. The formed LM was placed on the goniometer surface and was heated to 50^0 C. The buckling time for LMs formed by encapsulating water droplet in a closed chamber with constant temperature and humidity was noted and compared with that of LMs carrying H_2O_2 microdroplet. The buckling of formed marbles containing water droplet was measured and compared from their images with a calibrated scale using ImageJ software.

2. Results and Discussions

2.1 Selection of non-wetting powder for robust LMs

When a droplet of aqueous H_2O_2 (50% v/v) was dispensed onto the bed of magnesium silicate and, *Lycopodium* + talc mixture, the formation of LMs was observed due to hydrophobicity of the particles upon rolling. The stability of the marble formed using magnesium silicate was noted at time t = 30 s and 12 min, as shown in **Figure S1a** and **S1b** respectively. The droplet was rolled over the bed to ensure proper covering. Subsequently, a bed of *Lycopodium* + talc mixture was used to form the marbles and observed at time t = 30 s and 8 m, as shown in **Figure S1c** and **S1d** respectively. After 8 to 12 m, the micro-reservoirs of H_2O_2 formed using both the materials started evaporating rapidly that was indicated by a change in color.

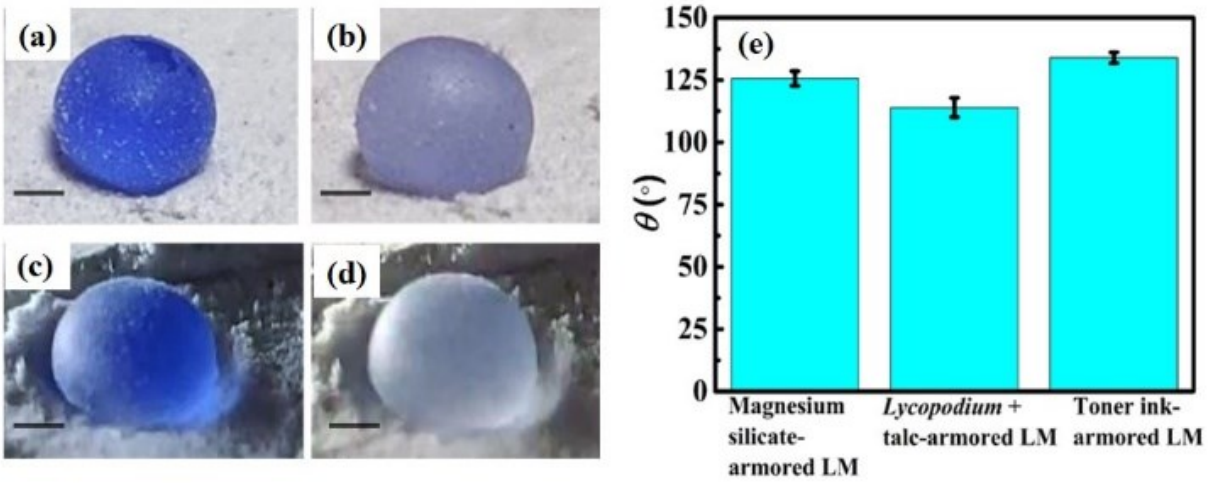

Figure S1. Fabrication of hydrogen peroxide (50% v/v) marble with time. Snapshots **(a)** and **(b)** shows the formation of marble on a bed of magnesium silicate at t = 30 s and t = 12 min respectively. Snapshots **(c)** and **(d)** show the profiles of marble on a bed of talc + *Lycopodium* at t = 30 s and t = 8 min respectively. Scale bar is 1 mm. **(e)** Contact angles (Θ) for magnesium silicate, *Lycopodium* grains + talc mixture and toner ink particles coating the LMs.

The magnetic fields do not exhibit any significant effect on LMs coated with *Lycopodium* and magnesium silicate due to their non-magnetic nature and instability. However, the hydrophobic coating of magnetic toner particles can be tailored to facilitate interactions with an external magnetic field. Out of these materials, it was observed that the toner ink armored-LMs was more robust; could transport H_2O_2 microdroplets easily without hindering its activity. No significant color change was observed for toner ink-armored LMs carrying microliters of H_2O_2 because of their superior robustness. The hydrophobic coating of particles offered a barrier effect for the evaporation of H_2O_2 droplet inside LMs which in turn decreased the evaporation rate and delayed time period. Hence, super hydrophobic toner ink was chosen to fabricate stable LMs for further experiments.

In order to test their hydrophobicity and robustness in correlation with toner ink-based formulations, comparative experiments were carried out. The hydrophobicity of magnesium silicate, *Lycopodium* grains plus talc mixture and toner ink particles coating the LMs was compared by measuring the apparent contact angles of liquid marbles against solid supports. As shown in **Figure S1e**, the contact angles (Θ) for magnesium silicate, *Lycopodium* grains + talc mixture and toner ink particles coating the LMs was found to be 125.14º, 113.43º and 133.7º respectively. Thus, the LMs coated with toner ink particles exhibited relatively greater hydrophobicity owing to their maximum contact angle.

The morphology of larger clumps of toner ink particles was observed by FESEM analysis revealing a granular mixture with 3–8 μm large toner clumps and small agglomerates with diameter 25–200 nm, as shown in **Figure S2a.** Therefore the material is a mixture of both micro and nanoparticles. SAED analysis revealed bright spots that indicated the crystalline nature of the toner due to the presence of crystalline iron particles, presented in **Figure S2b.**

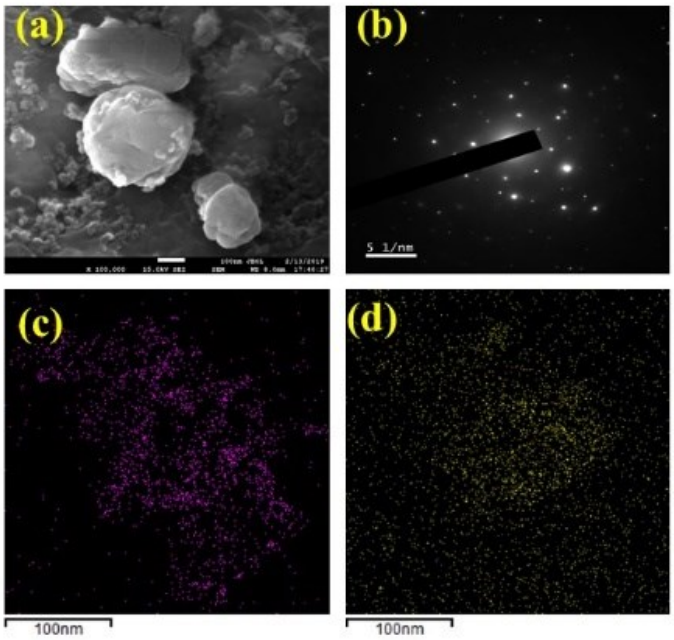

Figure S2. FESEM image **(a)** larger toner ink particles, scale bar 100 nm. **(b)** SAED analysis of toner ink particles. Elemental mapping of toner ink particles for the presence of **(c)** silicon and **(d)** carbon. Scale bar is 100 nm.

FETEM mapping confirmed that the silicon atoms were bonded to oxygen atoms and elemental carbon could be found everywhere in ample amount, as shown in **Figure S2c** and **Figure S2d**. From EDX analysis in **Figure S3a**, the atomic % of Fe, O, C and Si as 32, 37, 28 and 3% respectively. Whereas weight % of Fe, O, C and Si are 12, 21, 3 and 63% respectively. To facilitate electrostatic interaction, fluorescent bacterial cells was attached on the surface of toner ink by coating with CTAB.[3] Furthermore, the magnetization saturation for toner ink particles and CTAB-modified toner ink particles was measured by VSM analysis, as presented in **Figure S3b.** The magnetization saturation of toner ink particles was found to be 33.6 emu g^{-1}, which was reduced to 26.8 emu g^{-1} for CTAB-modified toner ink. Though a slight decrease in magnetic moment was observed after CTAB modification, the inherent magnetic response of modified toner was sufficient enough for toner ink-armored LMs to exhibit magnetic actuation.

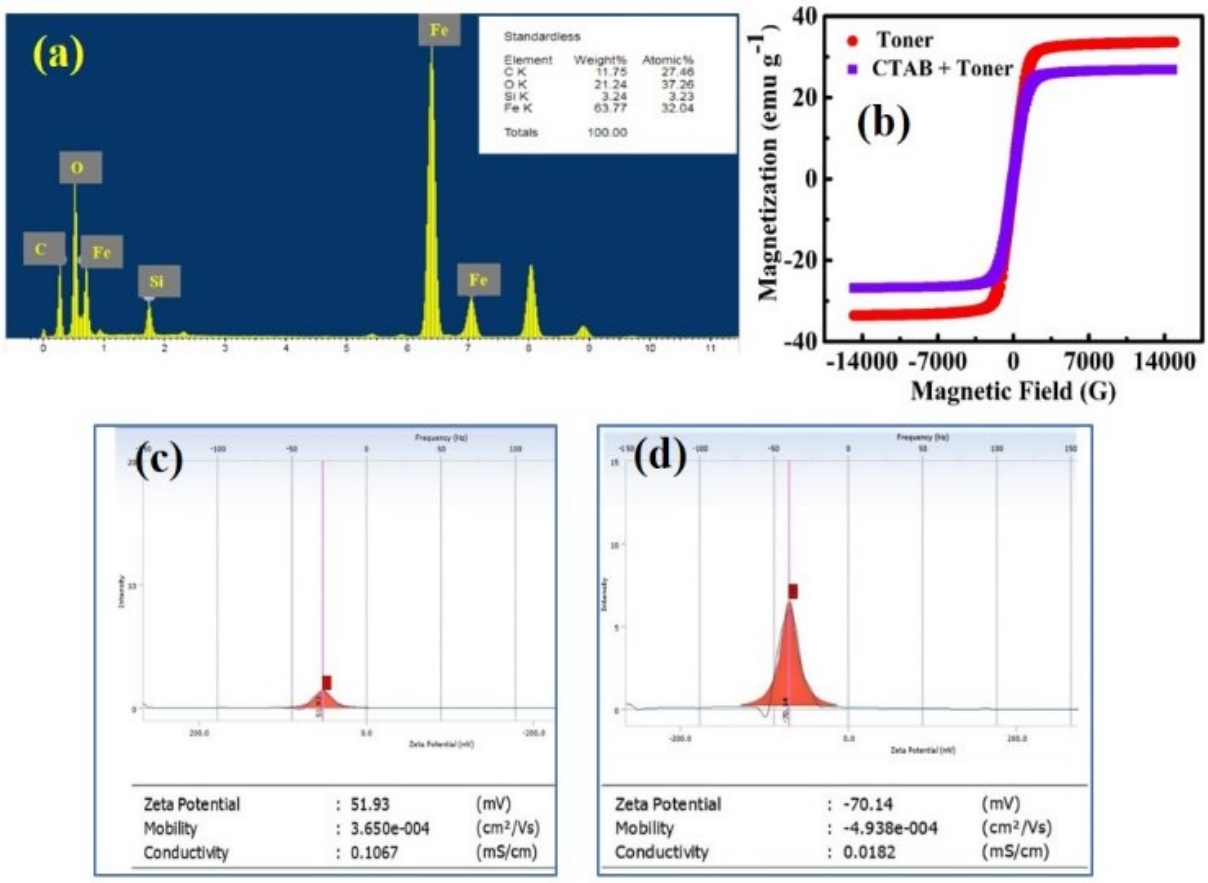

Figure S3. (a) EDX analysis of toner ink confirming the presence of Fe. **(b)** Magnetization curve of toner ink particles and CTAB-modified toner ink particles obtained using VSM. DLS analysis of **(c)** CTAB coated toner ink particles and **(d)** uncoated toner ink particles.

DLS analysis has been performed to find out the zeta potential of toner particles and CTAB coated toner particles, as shown in **Figure S3c** and **Figure S3d** respectively. The shift in zeta potential of LM after coating with CTAB solution was from -70 mV to 51.93 mV, which confirmed the coating of cationic CTAB on negatively charged toner particles. As the positively charged CTAB molecules binds to the negatively charged toner ink particles, the assembly structure of CTAB onto the surface of toner particles forms a complete hydrophobic monolayer. During this process, not only the positive charge on toner particles increases but also the surface hydrophobicity enhances.[4-6]

2.2 Iodometric Titration

The H_2O_2 droplet was mixed with H_2SO_4 that resulted in oxidation of iodide to iodine, shown in **Figure S4a**. The formation of iodine due to insufficient KI was confirmed by formation of a

black colored precipitate, displayed in **Figure S4b.** The homogenous solution of KI_3 has been presented in **Figure S4c** that was estimation by UV-Visible spectrophotometer. From the absorbance spectrum of tri-iodide ion, we observed that the maximum value of absorbance was obtained at wavelength of 285 nm.[7,8]

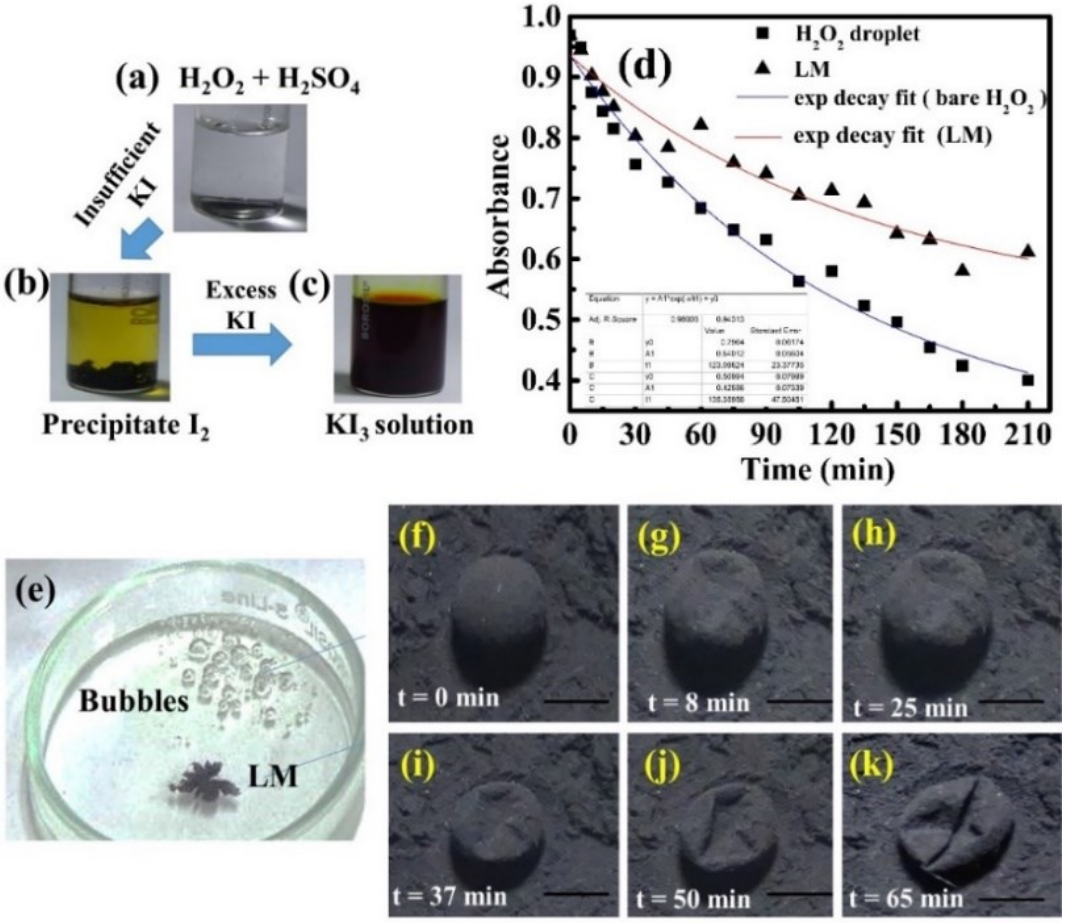

Figure S4. Photographs showing **(a)** addition of H_2O_2 solution to H_2SO_4 **(b)** formation of black precipitate of iodine due to insufficient KI **(c)** appearance of homogenous brown solution of potassium triiodide due to excess KI. **(d)** Variation of maximum absorbance with time for H_2O_2 droplet and liquid marble. **(e)** Snapshot showing evolution of oxygen bubbles when the marble is placed on a petridish containing KI solution, confirming the presence of stable H_2O_2 inside the marble. Sequence of top view frames **(f-k)** demonstrating the buckling time of water droplet illustrating evaporation with time, t = 0 min to 65 min. Scale bar is 1 mm.

The variation of absorbance maxima with respect to time for uncoated H_2O_2 droplet and LM has been represented in **Figure S4d.** The plot confirmed that toner ink armored LM shields the H_2O_2 droplet from decomposition, thus exhibiting lower rate of decomposition as compared to bare droplet. With time, the decrease of absorbance for bare H_2O_2 droplet was to a higher extent that proved the lower concentration of H_2O_2 in the droplet.

2.3 Stability of H_2O_2 inside the LM

The formed LM was stored to analyze the stability of H_2O_2 by placing it in a petridish containing 0.2 M KI solution. The marble immediately ruptured leading to outburst of H_2O_2 droplet. Being a strong catalyst, KI could decompose the microliter of H_2O_2 released from the droplet that was evident from the formation of oxygen bubbles in the petridish[9], as shown in **Figure S4e**. Therefore, the generation of bubbles indicated decomposition of H_2O_2 in the KI solution that confirmed the stability of the liquid stored inside the toner ink armored marble. This proved the efficacy of the LM to protect the reactive liquid from external surroundings.

2.4 Evaporation studies of water droplet

The evaporation behavior of individual micro-reservoirs of H_2O_2 droplet at of 50°C was compared with LMs carrying same volume of water droplet (20 µL). The buckling time for a LM containing water droplet started from 25 m and gradually reached maxima at 65 m with visible changes in diameter of the marbles, as shown in **Figure S4 (f-k)**. This proved a shorter lifetime for pure water droplets of similar volume since the droplet contained only water.[10, 11] Moreover, the buckling time for a LM containing H_2O_2 droplet started from 100 min and gradually reached maxima at 320 min [**refer Figure 7 (a-e)** of **manuscript**]. The results also revealed a shorter lifetime for LMs with H_2O droplets of similar volume as compared to LMs with H_2O_2 droplets. The boiling point of water is low due to the presence of weak hydrogen bonds. At 50°C, the water droplet evaporates at a higher rate due to low boiling point (100 ° C), thus causing rapid physical deformations of LMs with H_2O. On the contrary, LMs containing similar volume of H_2O_2 exhibits longer lifetime due to reduced evaporation rate owing to the higher boiling point of H_2O_2 (150.2 ° C).[12]

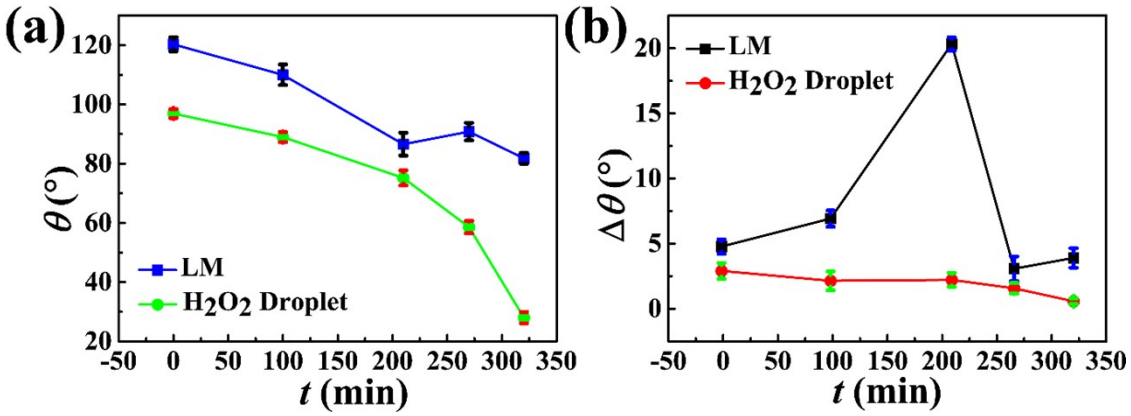

Figure S5. (a) The variation in contact angle (θ) of LM and H_2O_2 droplet with time. **(b)** The variation in contact angle hysteresis ($^{\Delta\theta}$) of LM and H_2O_2 droplet with time.

Further, the variation in contact angle (θ) and the contact angle hysteresis ($^{\Delta\theta}$) were investigated for LM and H_2O_2 droplet during evaporation. **Figure S5 (a)** shows that θ was gradually decreasing with time for both LM and H_2O_2 droplet during evaporation. However, the rate of the change of θ was higher for H_2O_2 droplet compared to LM because the rate of evaporation through the dense layer of hydrophobic toner ink - armored LM was lower as compared to the uncoated H_2O_2 droplet. **Figure S5 (b)** shows that $^{\Delta\theta}$ changed with time for both LM and H_2O_2 droplet during evaporation. $^{\Delta\theta}$ was calculated from the difference between advancing and receding angle of LM and H_2O_2 droplet. For H_2O_2 droplet, $^{\Delta\theta}$ monotonically decreased with time. However, for LM, $^{\Delta\theta}$ exhibited fluctuation because of the buckling and crumpling during evaporation.

2.5 Mathematical modelling for evaporation of LM

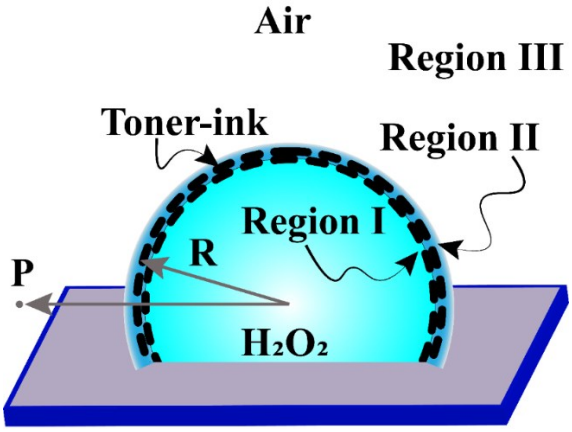

Figure S6. A schematic representation of toner ink-armored LM undergoing evaporation.

In order to model the evaporating toner ink-armored LM, we have considered three regions, i.e. region I (internal region of LM adjacent to toner-ink coating), region II (region of toner-ink coating on LM) and region III (air at a distance), as represented in **Figure S6**. As the thickness of the toner-ink is smaller as compared to the radius of the LM, region II is uniformly saturated with the vapor of H_2O_2 microdroplet entrapped inside LM. Therefore, the vapor molecules diffuses from region II to III due to evaporation. Subsequently, liquid molecules from region I fill up region II as vapor molecule to maintain the conservation of the mass. Therefore, a constant resistance can be observed during diffusion process from region II to III due to

evaporation. Hence, the mass flux around the LM at radial location (point P) can be illustrated as:

$$\dot{M}(r) = \dot{M}(r)\, w_A - \rho_{vap} D \, \mathrm{d}w_A / \mathrm{d}r \,. \quad (1)$$

Here $\dot{M}(r)$, w_A, ρ_{vap}, D and $\mathrm{d}w_A / \mathrm{d}r$ are defined as mass flux of liquid H_2O_2 vapour, mass fraction of liquid H_2O_2 vapour, density of liquid H_2O_2 vapour, diffusivity of liquid H_2O_2 in air, and gradient of mass fraction, respectively. **Figure S7** shows that the total mass of LM (M_{LM}) is the summation of the mass of hydrophobic coating (M_H), and mass of liquid H_2O_2 droplet (M_L).

$$M_{LM} = M_H + M_L \,. \quad (2)$$

Since the evaporation of LM with time promotes only the reduction in size, M_H is constant. So, rate of change in mass can be written as:

$$\dot{M}_{LM} = \dot{M}_L = 4\pi r^2 \dot{M}(r) \,. \quad (3)$$

After substituting equation (3) in equation (1), the final expression of mass faction at any point can be written as:

$$w_A = 1 - \left[(1 - w_A) \exp(-\dot{M}_{LM} / (4\pi \rho_{vap} D r)) / \exp(-\dot{M}_{LM} / (4\pi \rho_{vap} D R)) \right]. \quad (4)$$

Here, the boundary conditions are: $r = R$, $w_A = w_{AS}$, and $r = \infty$, $w_A = w_{A\infty}$. After applying the boundary conditions, the rate of change in mass of LM can be illustrated as:"

$$\dot{M}_{LM} = 4\pi \rho_{vap} D \ln \left[(1 - w_{A\infty}) / (1 - w_{AS}) \right]. \quad (5)$$

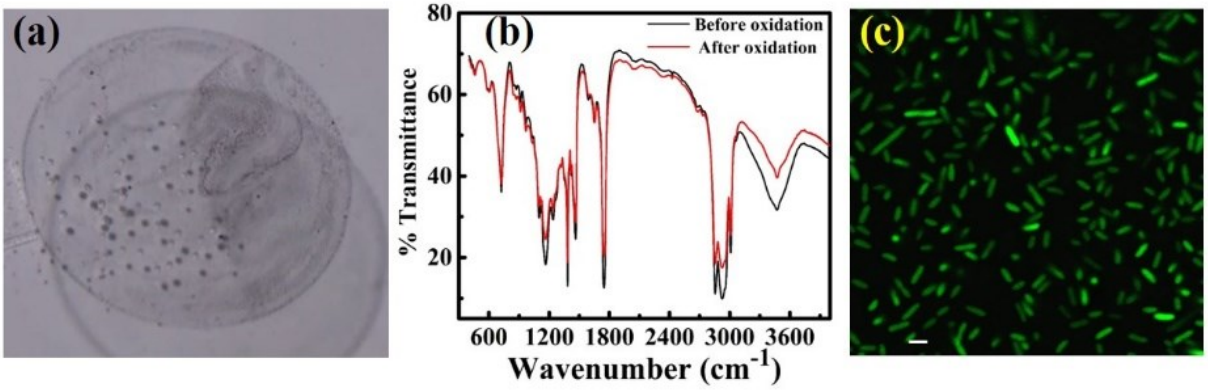

Figure S7. (a) Evolution of oxygen bubbles in oil due to destabilization of LM containing H_2O_2 droplet. **(b)** FTIR spectra of oil after and before oxidation. **(c)** CLSM image of control GFP expressing *E. coli* at 488 nm excitation wavelength. Scale bar is 1 μm.

Upon marble destabilization, the collected oil droplets were oxidized after decomposition of H_2O_2 droplet inside LM that was confirmed from the evolution of oxygen bubbles. The generation of oxygen bubbles in oil due to oxidation has been shown **Figure S7a.** The FTIR spectra of oil before and after oxidation in the wavenumber range of 3600-500 cm^{-1} has been shown in **Figure S7 b.** These spectra revealed the distinctive absorption bands for triglycerides present in oil.[13] The transmittance of light through the sample got increased after oxidation thereby implying the reduction in concentration.[14-16] Henceforth, this confirmed the oxidation of recovered oil by toner ink armored LM. The confocal image of control GFP expressing E. *coli* cells showing green fluorescence has been represented in **Figure S7c**.[17]

2.6 Antibacterial activity

The live untreated bacterial cells were examined using CLSM at an excitation wavelength of 488 nm. The antibacterial activity was investigated against GFP *E.coli* by treating them with different concentrations (40 to 160 µg mL^{-1}) of CTAB, LMs and CTAB-modified LMs (CTAB concentration ranging 40 to 160 µg mL^{-1}). Among different concentrations tested, the minimum concentration of CTAB, LMs and CTAB-modified LMs that measurably inhibited and killed the bacterial growth was considered as MIC and MBC respectively, represented in **Table S1.**

GFP E. coli	**(µg mL^{-1}) MIC**	**CTAB**	**LMs**	**CTAB-modified LMs**
		130	**114**	**87**

Table S1. MIC and MBC of samples against GFP expressing *E. coli* culture.

From the table, it could be interpreted that the MIC and MBC value of CTAB-modified LMs was far less indicating the synergistic antibacterial action involving CTAB coated LMs. The growth curve studies on GFP expressing *E.coli* indicated that at MIC (87 µg mL^{-1}) of CTAB-modified LMs, there was an arrest in bacterial growth and at its MBC (103 µg mL^{-1}), the bacterial colonies were completely killed. Comparatively, the free CTAB exhibited higher values of MIC and MBC of 130 µg $mL^{-1}$and 155 µg mL^{-1} respectively. The MIC and MBC values for LMs was found to be 114 µg mL^{-1} and 126 µg mL^{-1}, respectively.

Additionally, time-dependent real-time CLSM analysis of GFP *E.coli* attached on surface of CTAB-modified LMs was carried out by incubating the treated cells for a period of 1 h - 12 h and analysed under confocal microscope, ad shown in **Figure S8**. Time dependent bright-field, fluorescent and merged images were monitored after 1 h **(Figure S8 a-c)**, 3 h **(Figure S8 d-f)**, 6 h (**Figure S8 g-i)** and 12 h **(Figure S8 j-l)**. The images confirmed the attachment of GFP expressing *E. coli* bacteria on the surface of LMs and their subsequent killing. The strongest fluorescence was shown at 1 h indicating the presence of live bacteria on the LM surface. By contrast, the green fluorescence intensity of GFP expressing *E.coli* gradually decreased over time and showed negligible fluorescence after 12 h incubation. The decreasing intensity of GFP from *E. coli* attached on CTAB-modified LM surface acted as a visible marker, thus confirming time-dependent inhibition of bacterial growth and bactericidal effect.[17]

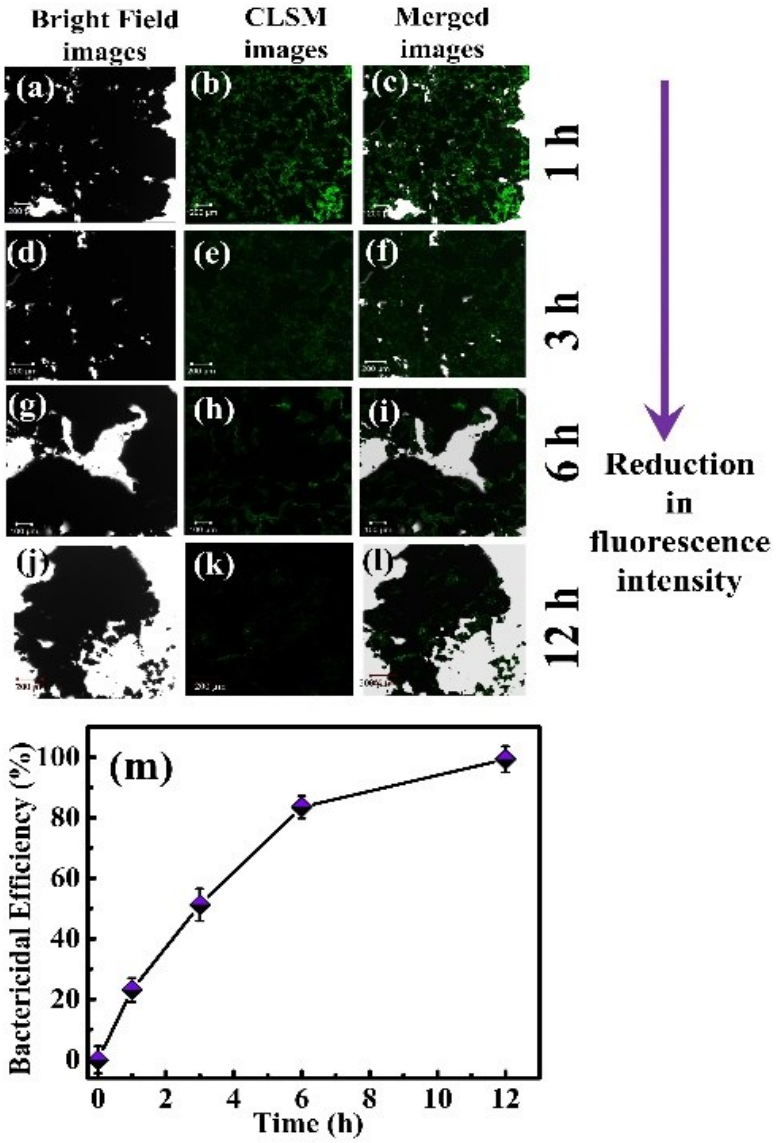

Figure S8. Bright-field, fluorescence, and merged confocal images of GFP *E.coli* attached on the surface of CTAB-modified LMs for a period of 1 h - 12 h at 37°C. **(a)** Bright-field **(b)** fluorescence, and **(c)** merged confocal images after 1 h incubation. Scale bar is 200 µm; **(d)** Bright-field **(e)** fluorescence, and **(f)** merged confocal images after 3 h incubation. Scale bar is 200 µm; **(g)** Bright-field **(h)** fluorescence, and **(i)** merged confocal images after 6 h incubation. Scale bar is 100 µm; **(j)** Bright-field **(k)** fluorescence, and **(l)** merged confocal images after 12 h incubation. Scale bar is 200 µm. **(m)** Bactericidal efficiency (%) studies by treating *E.coli* with CTAB-modified LM for 1 h - 12 h.

The bactericidal efficiency (%) was studied by treating GFP expressing *E.coli* culture with CTAB-modified LM and incubating the treated cells for a period of 1 h - 12 h. As displayed in **Figure S8 (m),** the bactericidal efficiency was observed to be 50% after incubating the treated cells for 4 h. However, with gradual increase in incubation time, the bactericidal efficiency was significantly elevated, reaching maxima of ~99.8% killing after incubating for 12 h. The

antibacterial efficacy of LMs was dependent on the incubation time that progressively increased with increase in exposure time. Thus, LMs strongly inhibited bacterial growth in the long term, producing largest toxic effect at 12th h. The above results could be related to the lowest intensity of green fluorescence that was detected by time-dependent CLSM analysis of LM-treated bacteria after 12 h incubation. Also, similar results were obtained from the lowest obtained MIC and MBC of CTAB-modified LM at the end of 12 h that displayed an enhanced antibacterial activity, correlative to minimum bacterial growth.

3 Supporting videos

Supporting video S1: The video shows the forced induced rolling of a toner ink armored LM (size ~2.5 mm) for storage and transport of 20 μL of H_2O_2 (50% v/v) droplet.

Supporting video S2: The video shows the reversible opening of pores on a toner ink armored LM (size ~2.5 mm) carrying H_2O_2 (50% v/v) droplet, under the action of an external magnetic force beneath the substrate.

Supporting video S3: The video shows the reversible closing of holes on a toner ink armored LM (size ~2.5 mm) carrying H_2O_2 droplet (50% v/v), upon removing the magnetic field.

Supporting video S4: The video shows the controlled propulsion of a toner ink armored LM (size ~3 mm) carrying H_2O_2 droplet (50% v/v) under the action of an external magnetic field.

Supporting video S5: The video shows the buckling of toner ink armored LM (size ~3 mm) at 50°C due to evaporation of encapsulated H_2O_2 droplet (50% v/v), measured using a Goniometer.

Supporting video S6: The video shows the buckling of uncoated H_2O_2 droplet (20 μL, 50% v/v) measured using a Goniometer.

Supporting video S7: The video shows the controlled magnetic actuation of "Marble in Oil" capsules (size ~3.5 mm) carrying H_2O_2 droplet (50% v/v) under the action of an external magnetic field by placing the marble in a petridish filled with 5 mL of water.

Supporting video S8: The video shows the collection of oil droplets from water by introducing a "Marble in Oil" capsule (size ~4 mm) into 5 mL of water in a petri dish and 20 μL of oil droplets. The motion of the capsule was controlled under the influence of a bar magnet.

Supporting video S9: The video shows in-situ oxidation of collected oil droplets using H_2O_2 droplet that generates oxygen bubbles in oil.

References

1. B. J. Deadman, K. Hellgardt and K. K. Hii, *React. Chem. Eng*., 2017, **2,** 462-466.
2. A. Hunter, *J. Bio. Chem*., 1910, **7,** 321-349.
3. C. A. Basar, A. Karagunduz, B. Keskinler and A. Cakici, *Appl. Surf. Sci*., 2003, **218**, 169–174.
4. R. Li, Z. Wang, X. Gu, C. Chen, Y. Zhang and D. Hu, *ACS Omega*, 2020, **5**, 4943-4952.
5. R. Songolzadeh and J. Moghadasi, Colloid. *Polym*. *Sci.,* 2017, **295**, 145–155.
6. C. A. Basar, A. Karagunduz, B. Keskinler and A. Cakici, *Appl. Surf. Sci*., 2003, **218**, 169–174.
7. A. E. Burgess and J. A. Davidson, *J. Chem. Educ*., 2012, **89**, 814−816.
8. S. H. Jung, J.W. Yeon, Y. Kang and K. Song, *Asian J. Chem*., 2014, **13**, 4084-4086.
9. M. Y. El-Sheikh, A. M. Habib, A. K. Abou-Seif and A. B. Zaki, *J Incl. Phenom*., 1986, **4**, 359-367.
10. C. Fullarton, T. C. Draper, N. Phillips, R. Mayne, B. P. J. de Lacy Costello and A. Adamatzky, *Langmuir*, 2018, **34**, 2573-2580.
11. K. R. Sreejith, C. Ooi, D. V. Dao, and N. T. Nguyen, R*SC Adv*., 2018, **8**, 15436-15443.
12. C. Hultman, A. Hill and G. McDonnell, *Pharm. Eng*., 2007, **27**, 22-32.
13. A. Rohman, *Int. J. Food Prop*., 2017, **20**, 1447-1456.
14. A. Rohman and Y. B Che Man, *Int. J. Food Prop*., 2013, **16**, 1594-1603.
15. L. Xu, T. Fei, Q. Li, X. Yu and Liu, L. *Anal. Methods*, 2015, **7**, 4328-4333.
16. M. Szmatoła, J. Chrobak, R. Grabowski, J. Iłowska, J. Woch, J. Szwach, I. Semeniuk, J. Drabik, M. Wrona, R. Kozdrach, B. Orlinska and M. Grymel, *Molecules*, 2018, **23**, 3243-3261.
17. R. Greenhalgh, M. Greenhalgh, F. Alshareef and G. D. Robson, *J. Microbial. Methods*, 2017, **141**, 67-72.